SGG≈SGS sc | nat

ORIGINAL PAPER

Open Access

Check for updates

The Twannberg iron meteorite strewn field in the Swiss Jura mountains: insights for Quaternary environmental conditions

Beda A. Hofmann[1,2*] , Naki Akçar[2], Sönke Szidat[3], Pierre G. Valla[4,2], Marcus Christl[5], Christoph Vockenhuber[5] and the Twannberg Search Team

Abstract

The ~ 10 km^2 strewn field of the Twannberg type IIG iron meteorite is located in the Swiss Jura Mountains, 30 km northwest of Bern. The strewn field has been mapped by a group of citizen scientists since 2006, yielding more than 2000 meteorite fragments with a total mass of 152.7 kg until the end of 2022. With a terrestrial age of 176 ± 19 ka and a minimum pre-atmospheric mass of ~ 250 t, the Twannberg meteorite is a local time marker in an area with a poorly-known paleoenvironmental history. The Twannberg strewn field is located just outside of the maximum extent of ice during the Last Glacial Maximum (LGM). On the Mont Sujet, meteorites are size-sorted in a 6-km long section of the primary strewn field (altitude 945–1370 m a.s.l.), indicating a fall direction from east-northeast to west-southwest (azimuth approximately 250°). On the Twannberg plateau and in the Twannbach gorge, meteorites are not size-sorted and occur in a ~ 5.7-km long area associated with till and recent stream sediments (altitude 430–1075 m a.s.l.). The mass distribution of meteorites on the Twannberg plateau demonstrate that these meteorites were not found where they fell but that they must have been transported up to several km by glacier ice flow after the fall. The distribution of meteorites and of glacially transported Alpine clasts on the Mont Sujet and on the Chasseral chain indicates the presence of local ice caps and of an approximately 200-m higher Alpine ice surface with respect to the LGM at the time of fall. This high ice level during MIS 6 (Marine Isotopic Stage 6, 191–130 ka) indicated by the meteorite distribution is consistent with surface exposure ages of 50–144 ka from nearby resting erratic boulders at altitudes of up to 1290 m a.s.l., including the newly dated Jobert boulder (63 ka). These boulders indicate an ice level ~ 400 m higher than during LGM at a time not later than MIS 6. Post-LGM luminescence ages of loess-containing meteorites on the Mont Sujet and ^{14}C ages of materials associated with meteorite finds indicate relatively young pedoturbation and increased oxidation of meteorites since ~ 7300 cal BP, possibly correlated with deforestation and enhanced erosion resulting from increased human activities since the Neolithic. This study shows that Twannberg meteorites in their palaeoenvironmental context provide valuable information about ice levels and transport directions during MIS 6 and about their interaction with the post-LGM environmental conditions. The unique Twannberg strewn field has the potential to reveal more valuable information.

Keywords Twannberg iron meteorite, Swiss Jura mountains, Meteorite strewn field, Alpine glaciations, Paleo-glacial reconstruction, Geochronology

---

*Correspondence:
Beda A. Hofmann
beda.hofmann@unibe.ch
Full list of author information is available at the end of the article

Springer Open

1 Introduction

Numerous strewn fields resulting from the disruption of meteorites in the atmosphere during entry are known, but only few have been mapped in detail (Kring et al., 2001; Gnos et al., 2009; Popova et al., 2013). Iron meteorite strewn fields are relatively rare and often associated with small impact craters. Such events with well-known meteorite distributions are Sikhote Alin (Krinov, 1974),

Henbury (Buhl & McColl, 2012), Whitecourt (Kofmann et al., 2010) and Gebel Kamil (Folco et al., 2011). The Twannberg strewn field, located in the Swiss Jura Mountains 3–10 km west of the city of Biel and 30 km northwest of Bern (Fig. 1a) is unique as it is the only well-documented strewn field of an iron meteorite of the rare type IIG (Wasson & Choe, 2009). IIG irons are structurally hexaedrites, lacking the Widmanstätten pattern
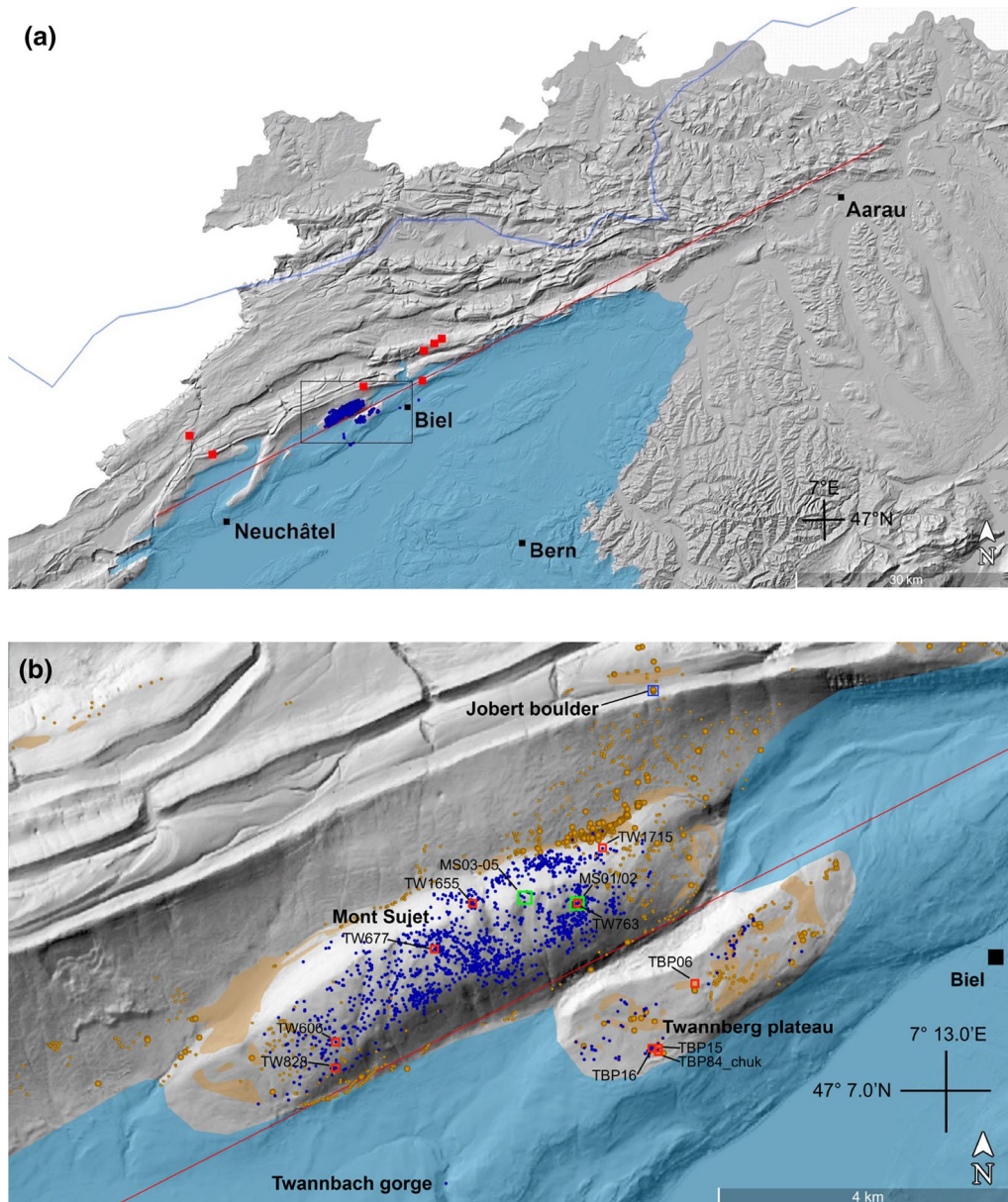
Fig. 1 a Overview of the study area in Switzerland. The box is the Twannberg area shown in detail in Fig. 2 with meteorite find locations. The red line corresponds to the profile shown in Fig. 7. Maximum Alpine ice extent (Bickel et al., 2015, blue line) and LGM (Schlüchter, 2009, blue area) are shown for reference. Red squares are exposure-dated pre-LGM boulders. **b** The Twannberg area with meteorite finds (blue dots) and extent of LGM ice (light blue area). Yellow symbols show distribution of pre-LGM glacially transported Alpine material (areas = till, large circles = boulders, small circles = clasts). LGM ice limit based on Schlüchter (2009) and Aufranc and Burkhalter (2017). Square symbols indicate the locations of dated samples

typical of octahedrites, and are characterized by the lowest nickel content (~ 4.5 wt.% Ni in metal) among all iron meteorites. Including Twannberg, only six different IIG iron meteorites are officially named (Meteoritical Society database, https://www.lpi.usra.edu/meteor/). The find locations of 2088 individual meteorites with a total mass of 152.7 kg have been mapped until end of 2022. Twannberg is one of the largest iron meteorite strewn fields. After the first chance find of a 15.9 kg mass in 1984 (Bühler, 1986), many additional finds were made from 2000 on (Hofmann et al., 2009, 2016; Smith et al., 2017). Finds of meteorites were made in three areas (Fig. 1b): (i) the Twannberg plateau located on the southernmost anticlinal fold of the Jura Mountains in the area where the first, name-giving meteorite was found; (ii) the Mont Sujet, a ~ 7 km long anticlinal fold; and (iii) the Twannbach gorge, a canyon cutting through the southernmost anticline. Previous studies investigated the mineralogy, chemical composition, cosmic-ray exposure history and terrestrial age of the Twannberg meteorite (Hofmann et al., 2009; Smith et al., 2017, 2019). The spatial extension of the strewn field has been systematically mapped since 2009 by the Twannberg search team, a group of 15–30 citizen-scientist meteorite hunters (see acknowledgments for details).

The currently mapped part of the Twannberg strewn field is located beyond the limit of the LGM extent of the Valais glacier at ca. 24 ka (Fig. 1b; Schlüchter, 2009; Graf et al., 2015; Ivy-Ochs, 2015). The strewn field is located on the southernmost two anticlines of the folded Jura Mountains, made up mainly of Upper Jurassic limestones and marls with some Miocene sediments preserved in synclines (Aufranc & Burkhalter, 2017). Anticlinal mountain chains of the folded Jura reach a maximum elevation of 1606 m at Chasseral in the study area, with steadily declining altitudes towards northeast. Glacial drift and till of Alpine origin including key lithologies of the Valais glacier (Allalin metagabbro, eclogites, magnetite ore and Carboniferous conglomerates) occur beyond the maximum limit of LGM ice distribution, typically at altitudes of up to around 1150–1200 m a.s.l., but locally up to 1320 m a.s.l. near the strewn field area. Higher areas up to 1600 m a.s.l. are generally free of Alpine clasts. The presence of Alpine boulders at high altitude in the Jura Mountains provides evidence of minimum ice-surface elevation during pre-LGM glaciations (e.g. Heim, 1919; Graf et al., 2015), but these glaciations are poorly constrained. Surface exposure ages of boulders located at altitudes from 1040 to 1260 m a.s.l. on Mont Montoz (14 km northeast of the strewn field) and on Mont d'Amin and near La Chaux-de-Fonds (18–21 km southwest) yielded ages between 50 ± 2 and 144 ± 5 ka, which are interpreted as a result of reworking by local LGM

glaciers of boulders transported during a more extensive glaciation prior to MIS 6 (Marine Isotopic Stage 6, 191–130 ka; Graf et al., 2007, 2015). Alternatively, these ages have been interpreted as evidence of a higher ice surface during the penultimate glaciation by Gruner et al. (2013). An age of 500 ± 100 ka for the Most Extensive Glaciation in the northern Alpine Foreland was recently suggested by Dieleman et al. (2022) based on isochron-burial dating of the Bünten Till (20 km east of Basel). Besides these studies, direct age constraints for pre-LGM alpine glaciations in the Jura Mountains are currently absent.

With a terrestrial age of 176 ± 19 ka based on $^{41}Ca/^{36}Cl$ and supported by less accurate ages based on $^{36}Cl/^{26}Al$ and $^{36}Cl/^{10}Be$ (Smith et al., 2017, 2019, Additional file 1: Material S1), the Twannberg meteorite strewn field provides a local marker of MIS 6 age in the Swiss Jura Mountains where pre-LGM glaciation history is poorly constrained. The characteristic type IIG meteorite fragments allow unambiguous identification and their large number (>2000) renders fragments of the Twannberg meteorite easily identifiable markers. We use these to unravel the glaciation history of the fall area, providing constraints for the ice extent during the MIS 6 and an explanation for the spatial distribution of Twannberg meteorite finds. Luminescence and ^{14}C dating constraints on loess-type soils on the Mont Sujet and meteorite-associated organic material provide information about processes that occurred long after the fall, after the end of the LGM.

2 Methods

2.1 Strewn-field mapping and –orientation

The distribution of meteorites is based on meteorite search using handheld metal detectors and in part (Twannbach gorge) using strong magnets. Each find is documented with GPS coordinates, depth of find and date. All finds of meteorites and suspected meteorites were analyzed by X-ray fluorescence using a NITON GOLDD+instrument, allowing rapid discrimination between meteorites (typically >0.5 wt% nickel in the oxidized surface) and man-made iron (typically <0.1 wt% nickel). In case of doubt, cut surfaces were analyzed in addition and some samples were identified by X-ray tomography showing the characteristic large skeletal schreibersites. All samples were inspected under binocular lenses for presence of fusion crust and adhering sediment material and organic matter. Data for all recovered samples of the Twannberg meteorite are available from the database of the Meteoritical Society: https://www.lpi.usra.edu/meteor/metbull.php

Alpine glacial drift material was mapped during meteorite searches. In addition, soil samples of several kg were taken in areas lacking information and wet-sieved

to obtain a fraction > 1 mm to search for Alpine drift. The fall direction of the Twannberg strewn field was estimated by finding the direction of strongest decrease of log mass versus distance, for series of parallel stripes of 200-m width covering all Mont Sujet finds. Details for this procedure are given in the Additional file 1: Material S2.

2.2 Surface exposure dating

Following the sampling strategy used in previous studies (e.g., Akçar et al., 2011), the Jobert boulder, which is the largest erratic boulder (5 × 3 × 2 m) in the study area near the Ferme Jobert (Jobert farm) at an altitude of 1290 m a.s.l., was sampled for the analysis of cosmogenic ^{10}Be and ^{26}Al using a portable drill, hammer and chisel (cf. Akçar et al., 2011). The sampled top boulder surface was 2.5 m above the surrounding ground. The sampling of the protected block at 47° 9.953'N 7° 10.581'E (see Fig. 1b) was performed on August 28, 2017, with permission of the "Abteilung Naturförderung" of the Canton of Bern. Sampling documentation is provided in the Additional file 1: Material S3. A reference rock sample is stored at the Natural History Museum Bern, Inv. Nr. 43393. For the isolation of quartz from the rock sample, a modified version of the technique described by Kohl and Nishiizumi (1992) was used (Akçar et al., 2017).

Cosmogenic ^{10}Be and ^{26}Al were extracted following the laboratory protocol of Akçar et al. (2012) at the Surface Exposure Laboratory of the Institute of Geological Sciences at the University of Bern. $^{10}Be/^9Be$ and $^{26}Al/^{27}Al$ ratios were determined by the 0.5 MV TANDY AMS facility in ETH Zurich (Christl & Kubik, 2013; Kubik & Christl, 2010). The measured $^{10}Be/^9Be$ ratio was corrected by applying a long-term weighted average full process blank ratio of $(2.37 \pm 0.62) \times 10^{-15}$. The total Al concentration of the sample was measured by inductively coupled plasma optical emission spectrometry (ICP-OES) at the Institute of Geological Sciences of the University of Bern. The $^{26}Al/^{10}Be$ ratio of the analyzed sample was calculated using the CRONUS-Earth exposure age calculator, and referenced to 07KNSTD (Balco & Rovey, 2008, and the update from v. 2.2 to v. 2.3 published by Balco in June 2016; http://hess.ess.washington.edu/math/v. 2.3). Cosmogenic ^{10}Be and ^{26}Al exposure ages were computed with the online exposure age calculator formerly known as the CRONUS-Earth online calculator (http://hess.ess.washington.edu/math/v3/; Balco & Rovey, 2008) by using the time-dependent Lal 1991/Stone 2000 scaling scheme. In the age calculations, half-lives of 1.39 Ma for ^{10}Be (Chmeleff et al., 2010; Korschinek et al., 2010) and 0.71 Ma for ^{26}Al (Norris et al., 1983; Nishiizumi, 2004) were used. In addition, topographic shielding (based on Dunne et al., 1999), sample thickness (using an

exponential attenuation length of 160 g/cm^2), and rock density (2.65 g/cm^3) were accounted for. No correction for erosion and snow cover was applied.

2.3 Luminescence dating

Five fine-grain samples were collected for luminescence dating from the loess-type soils on the Mont Sujet on June 17, 2017, along a hillslope (MS-01 and -02) and on the plateau (MS-03 to -05, Fig. 1b). Samples were collected with opaque plastic tubes pounded into fresh sediment surface, and have been prepared at the Institute of Geological Sciences (Univ. Bern) following the protocol described in Serra et al. (2021). Under subdued laboratory illumination, samples were treated with HCl (32%) and H_2O_2 (30%) to remove carbonates and organic components, respectively. Sedimentation in Atterberg cylinders (based on Stokes' Law) was used to extract the 4–30 μm grain size fraction. Polymineral separates were settled on 10-mm diameter stainless steel discs for subsequent luminescence analyses.

All luminescence measurements were carried out using TL/OSLDA-20 Risø readers, equipped with a calibrated $^{90}Sr/^{90}Y$ beta source (Institute of Geological Sciences, Univ. Bern). Luminescence signals were detected using an EMI 9235QA photomultiplier tube, in the blue region through a Schott BG-39 and L.O.T.-Oriel D410/30 nm filter combination, for polymineral InfraRed-Stimulated Luminescence (IRSL) measurements. We used the post-IR IRSL protocol of Buylaert et al. (2009), applying first a preheat treatment at 250 °C for 60 s before a single-aliquot regenerative-dose (SAR) protocol (Murray & Wintle, 2000) with a first IRSL stimulation at 50 °C (100 s, IR50) followed by a second IRSL stimulation at 225 °C (100 s, pIR225). For all the samples, residual doses and dose recovery ratios were quantified. Dose–response curves were constructed using an exponential + linear fitting (with recycling ratios within 10% of unity and recuperation within 5% of the natural dose used as acceptance criteria for the single-aliquot data). About 400 g of bulk sediment material was collected from the surrounding of each sample to determine the environmental dose rate. The material was desiccated at 60 °C to enable water content quantification. U, Th and K activities were measured using high-resolution gamma spectrometry (Department of Chemistry and Biochemistry, Univ. Bern; Preusser & Kasper, 2001) and were employed, together with the measured water content, as inputs for final dose rate determination through the Dose Rate and Age Calculator (DRAC; Durcan et al., 2015).

We used the Luminescence R package (Kreutzer et al., 2012) to quantify the Central Age Model (CAM) for all samples (Galbraith et al., 1999), given the low measured overdispersion between aliquots. Fading rates (g2days)

were measured following Auclair et al. (2003). Final fading-corrected ages were calculated following the fading correction procedure of Huntley and Lamothe (2001).

2.4 ¹⁴C dating

¹⁴C-dating was performed at the Laboratory for the Analysis of Radiocarbon with AMS (LARA) at the University of Bern, using the method described in Szidat et al. (2014). Charcoal samples from soils and samples of visually apparent rust-impregnated wood in the oxide (rust) crust of meteorites were mechanically isolated and pretreated with 20% HCl to remove iron hydroxides/carbonates, followed by treatment with 10% H_2O_2 to remove possible organic contaminants. The sample of chukanovite was mechanically extracted from a sample of the oxide crust of meteorite sample TW84. Calendar ages were determined from the measured ¹⁴C ages using the IntCal20 calibration curve with the NH Zone 1 addition (Hua et al., 2013; Reimer et al., 2020).

3 Results

3.1 Strewn-field documentation

The distribution of meteorite finds and the mass distribution data (Figs. 1b, 2, 3, 4, Table 1) show that finds on the Mont Sujet are most numerous, cover the largest

area and mostly occur in an area essentially devoid of Alpine drift material. Meteorites found on the Mont Sujet (median mass 25 g, range 0.064–1407 g) show a clear size sorting with a mass increase from the northeast to the southwest of 0.24 log mass (g) per km (Fig. 2). Mont Sujet meteorites typically are well preserved, many of them showing regmaglypts. Further proof of the preservation of the original shape and mass is the common occurrence (14.5% of samples) of remnants of the fusion crust including flow lines (Fig. 5). On the Mont Sujet, there are zones both in the southwest and the northeast where meteorites and Alpine clasts occur in the same area (altitude 945–1150 m a.s.l., with few pebbles occurring higher). The central part of the Mont Sujet (approx. 80% of the area) is free of Alpine pebbles. On the Twannberg plateau and in the extreme northeast of the Mont Sujet, meteorites (median mass 57 g, range 3.4–15,915 g) are closely associated with till rich in Alpine material and quartz/silicate grains are often attached to meteorites by weathering-derived iron hydroxides (57% of samples). Size and distribution of meteorites do not show a size trend (Fig. 2). Only a single meteorite (1.3% of samples) with fusion crust and flow lines under attached till material has been found on the Twannberg plateau
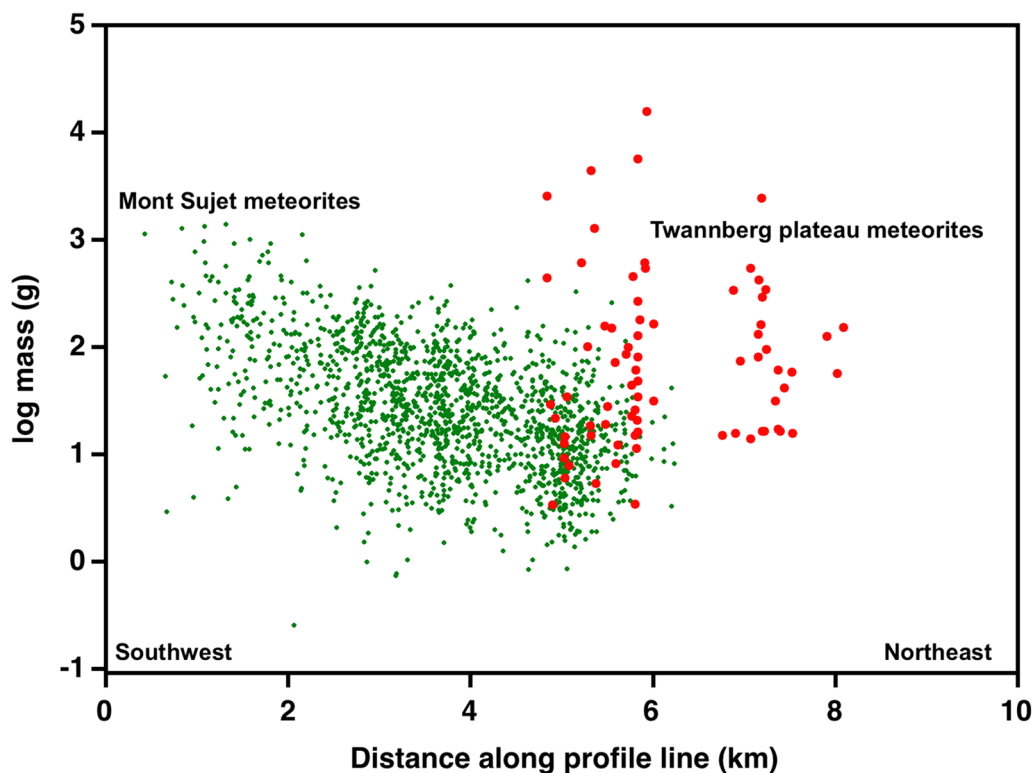
Fig. 2 Log mass (g) of Twannberg meteorites projected on the profile line shown in Fig. 1a, b. Note the systematic decrease of mass (0.24 log mass units/km) from SW to NE on the Mont Sujet, while Twannberg plateau meteorites are generally larger and do not show any size trend
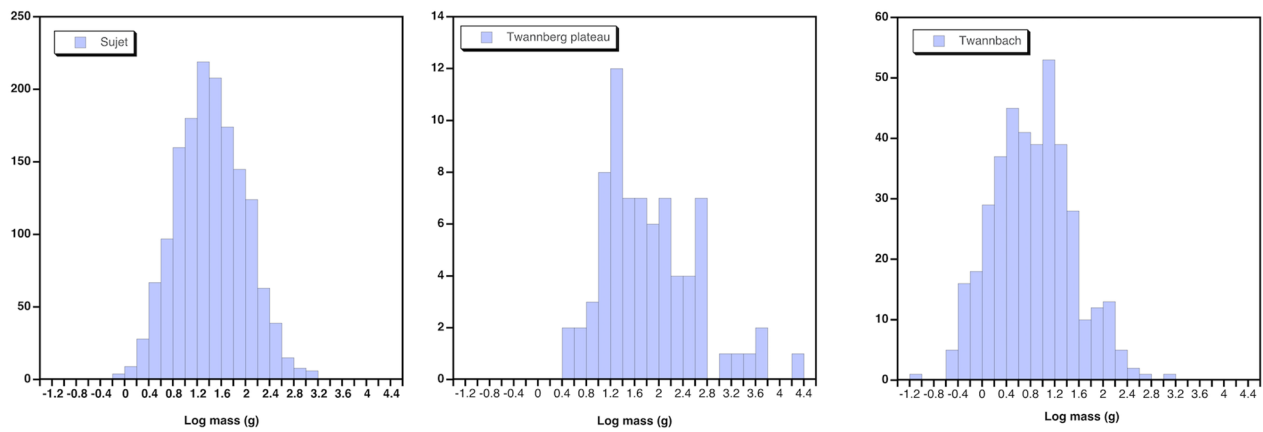
Fig. 3 Histograms of meteorite mass distributions of the populations from Mont Sujet, Twannberg plateau and Twannbach gorge
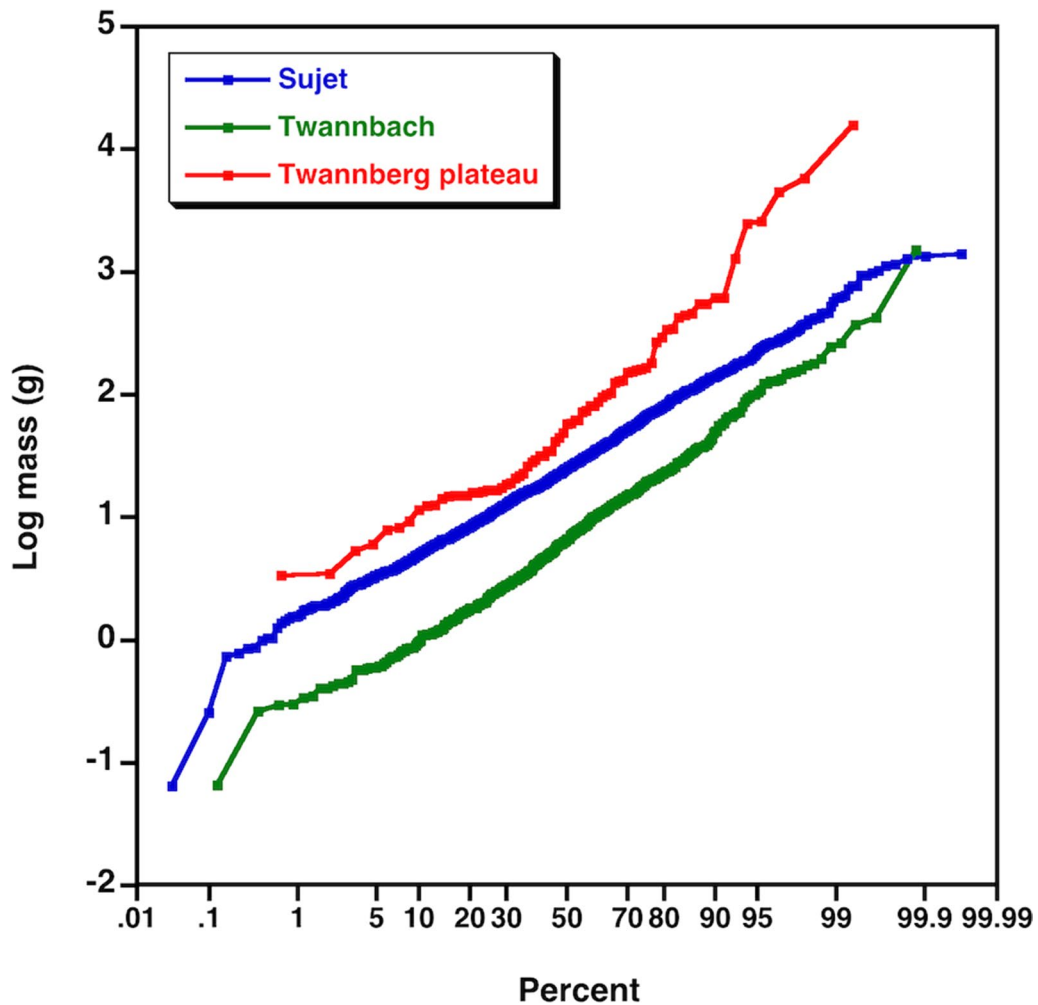
Fig. 4 Cumulative mass-frequency plot for meteorite populations from Mont Sujet, Twannberg plateau and Twannbach gorge

Table 1 Characteristics of different meteorite populations

|	Twannberg plateau	Mont Sujet	Twannbach gorge
Number of meteorite samples	75	1619	391
Average mass (g)	534	60.2	24.6
Median mass (g)	57.2	25.2	6.7
Largest mass (g)	15915	1407	1521
Smallest mass (g)	3.4	0.064	0.066
Total mass (kg)	40.49	97.46	9.72
% with fusion crust/flow lines	1.3	14.5	0.0
% with attached glacial material	57.3	2.5	34.3
% with attached plant material	8.0	4.8	0.0

All meteorites found between 1984 and end of 2022 are considered, n = 2088, including three from unknown locations

(Fig. 6). In the Twannbach gorge, meteorites are generally small (median mass 6.7 g, range 0.066–1521 g) and often show adhering material derived from till rich in Alpine clasts. The grinding effect of fluvial transport typically affected both the oxidation rind and till-derived Alpine clastic material attached to meteorites by oxidation products. The Twannbach Gorge is the only meteorite-find area previously occupied by the LGM glaciers. A linear regression of all find coordinates

on the Mont Sujet corresponds to an azimuth of 243° while the direction of maximum mass decrease of all meteorites has an azimuth of 241°, essentially corresponding to the elongation of the Mont Sujet anticline (∼242°). The latter values may be misleading if an elongated section of a strewn field is preserved with an elongation axis transverse to the strewn field axis. Using an approach of segmentation of the strewn field find location data into 200-m wide stripes and rotating these (see Additional file 1: Material S2), the direction of steepest slope of log mass of meteorite masses yields an azimuth of 252°, about 10° different from the apparent direction. However, a considerable uncertainty must be assigned to this value. We consider a fall azimuth of 250 ± 20° as the currently best approximation for the direction of fall.

3.2 Exposure age of the Jobert erratic boulder

The accelerator mass spectrometry analysis of the cosmogenic ^{10}Be and ^{26}Al yielded concentrations of $(75.18 \pm 1.13) \times 10^4$ at/g and $(524.21 \pm 6.47) \times 10^4$ at/g, respectively (Table 2). The calculated apparent ^{10}Be and ^{26}Al exposure ages are 63.1 ± 1.0 ka and 63.7 ± 0.8 ka (internal errors). The identical ages and the ^{26}Al/^{10}Be ratio of 6.97 ± 0.14 indicate a simple exposure history (cf. Halsted et al., 2021).
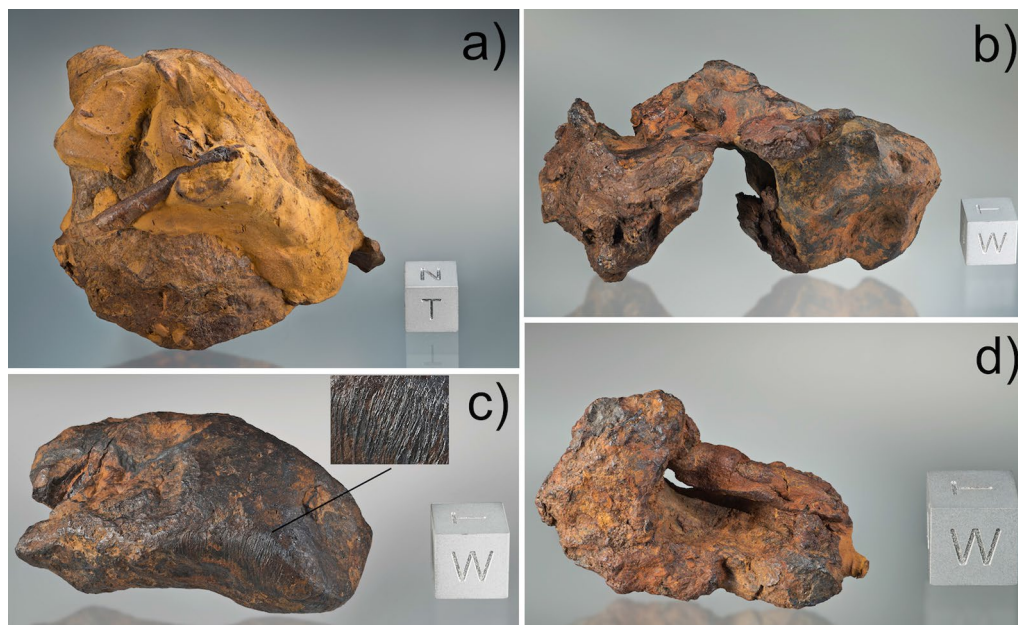
Fig. 5 Twannberg meteorites from Mont Sujet. **a** TW763 showing adhering soil with wood remnants (^{14}C age 2943–2796 cal BP), found by Gino Bernasconi; **b** TW1655 with attached wood remnants on top (^{14}C age 1865–1626 cal BP), found by Manuel Eggimann; **c** TW1727 with preserved flow lines; inset shows details of low-lines (5 mm width), found by Fritz Weber; **d** TW1715 with iron-hydroxide-impregnated wood remnant (^{14}C age 5575–5045 cal BP), found by Beda Hofmann. Edge of cube = 1 cm in all images. Photo credit: Thomas Schüpbach

3.3 Luminescence ages of loess-type soils

Loess-type soils at two locations of meteorites finds on Mont Sujet (Tables 3, 4) yielded luminescence ages between 3.5 ± 0.4 and 15.1 ± 1.0 ka. Out of five samples taken at two meteorite-find localities, three samples turned out to be disturbed by post-deposition slope processes. Both these samples were taken at a sloping site (MS-01 and -02) and the shallowest of three samples taken at a horizontal site (MS-05). After the exclusion of disturbed samples, two samples yielded consistent IR50 and pIR225 ages of 10.9 ± 0.7 to

Fig. 6 Twannberg mass TW934. This meteorite specimen with adhering till material was found on the Twannberg plateau. Left image shows complete specimen. Edge of cube = 1 cm. Right image shows detail with well-preserved fusion crust and flow-lines. Preservation of fusion crust indicates gentle transport on the glacier. Found by Marcel Häuselmann. Photo credit: Thomas Schüpbach

Table 2 Cosmogenic ^{10}Be and ^{26}Al results for the Jobert boulder sample

Sample name	Quartz dissolved (g)	^{9}Be Spike (mg)	^{10}Be ($\times 10^4$ at/g)	Total Al (mg)	^{26}Al ($\times 10^4$ at/g)	^{26}Al/^{10}Be
JOBE-1	49.8431	0.1998	75.18 ± 1.13	2.03	524.21 ± 6.47	6.97 ± 0.14

Accelerator mass spectrometry (AMS) measurement errors are at 1 s level, including the statistical (counting) error and the error due to normalization of standards and blanks. The error weighted average ^{10}Be/^{9}Be full-process blank ratio is $(2.37 \pm 0.62) \times 10-15$. ^{26}Al/^{10}Be ratios were calculated with the CRONUS-Earth exposure age calculator and were referenced to 07KNSTD (http://hess.ess.washington.edu/math/(v.2.3); Balco & Rovey, 2008 and update from v. 2.2 to v. 2.3 published by Balco in June 2016)

Table 3 IRSL dating of loess-type soils of Mont Sujet

Sample (*aliquots*)	Signal	Dose recovery ratio[1]	Residuals[1] (Gy)	CAM[2] uncorrected D$_e$ (Gy)	OD[2] (%)	Fading[4] g$_{2days}$ (%/decade)	CAM fading-corrected age (ka)
MS-01 (*6*)	IR50	0.93 ± 0.02	0.8	12.8 ± 1.0	6.6	2.5 ± 0.3	3.5 ± 0.4
	pIR225	1.10 ± 0.02	4.9	32.9 ± 0.8	4.4	0.7 ± 0.3	7.1 ± 0.5
MS-02 (*7*)	IR50	0.93 ± 0.05	0.6	17.9 ± 0.3	0.1	2.4 ± 0.3	5.0 ± 0.3
	pIR225	0.99 ± 0.01	3.6	40.7 ± 1.2	7.3	0.6 ± 0.3	9.2 ± 0.7
MS-03 (*8*)	IR50	1.07 ± 0.2	0.9	43.7 ± 0.9	4.5	2.6 ± 0.2	12.3 ± 0.8
	pIR225	1.19 ± 0.04	8.0	69.4 ± 2.2	7.9	0.8 ± 0.2	15.1 ± 1.0
MS-04 (*8*)	IR50	0.95 ± 0.02	0.9	39.3 ± 0.7	3.3	2.5 ± 0.2	10.9 ± 0.7
	pIR225	1.03 ± 0.01	5.1	58.0 ± 1.4	5.2	0.8 ± 0.2	13.0 ± 0.8
MS-05 (*7*)	IR50	0.94 ± 0.01	0.8	18.6 ± 0.6	6.9	2.1 ± 0.3	4.9 ± 0.4
	pIR225	1.12 ± 0.02	5.3	36.5 ± 1.2	7.3	0.8 ± 0.3	7.7 ± 0.6

IRSL dating of the loess-type soils of Mont Sujet on fine-grain small-aliquots, using feldspar infra-red luminescence at 50 °C (IR50) and post-infra-red infra-red luminescence at 225 °C (pIR225) signals. Analytical details and measurement protocols are given in the main text

[1] Dose recovery ratios have been calulated for each individual sample and using a given dose of 30 Gy for 5 aliquots. Residuals have been estimated for 4 aliquots per sample and are substracted to De for age determination

[2] De = Equivalent doses (non-corrected for residuals), *CAM* Central Age Model, *OD* overdispersion of D$_e$ distribution (Galbraith et al., 1999)

[3] Fading measurements have been performed on all aliquots per sample to evaluate the variability in fading rates for IR50 and pIR225 signals

Table 4 Details of dose-rate calculations for IRSL dating

Sample	Coordinates (WGS84, °N/°E, and elevation, m a.s.l.)	Radionuclide concentration[1]			Depth below surface (m)	Total dose rate[2] (Gy ka^{-1})
		U (ppm)	Th (ppm)	K (%)		
MS-01	47.14015/7.1628333/1280	4.76 ± 0.24	13.93 ± 0.70	1.06 ± 0.05	0.30 ± 0.05	4.21 ± 0.23
MS-02	47.14015/7.1628333/1280	4.76 ± 0.24	13.93 ± 0.70	1.06 ± 0.05	0.40 ± 0.05	4.21 ± 0.23
MS-03	47.14135/7.1568/1330	4.66 ± 0.23	12.34 ± 0.62	1.46 ± 0.07	0.40 ± 0.05	4.35 ± 0.23
MS-04	47.14135/7.1568/1330	4.66 ± 0.23	12.34 ± 0.62	1.46 ± 0.07	0.40 ± 0.05	4.35 ± 0.23
MS-05	47.14135/7.1568/1330	4.66 ± 0.23	12.34 ± 0.62	1.46 ± 0.07	0.20 ± 0.05	4.34 ± 0.23

[1] Radionuclide concentrations were quantified on bulk samples using high-resolution gamma spectrometry (Department of Chemistry and Biochemistry, Univ. Bern)

[2] Dose rate calculations were performed with DRAC (Durcan et al., 2015), assuming water content of 25 ± 2% and bulk sample density of 2.3 g cm^{-3}, an internal K-content of 12.5 ± 0.5% (Huntley & Baril, 1997) and an alpha efficiency value of 0.15 ± 0.05 (Balescu & Lamothe, 1994). Sampling location for MS-01/02 corresponds to find location of meteorite TW763. Sampling location for MS-03/04/05 corresponds to find location of meteorite TW141

13.0 ± 0.8 ka (Table 3, Fig. 7), evidencing that the age of the thin loess cover is post-LGM.

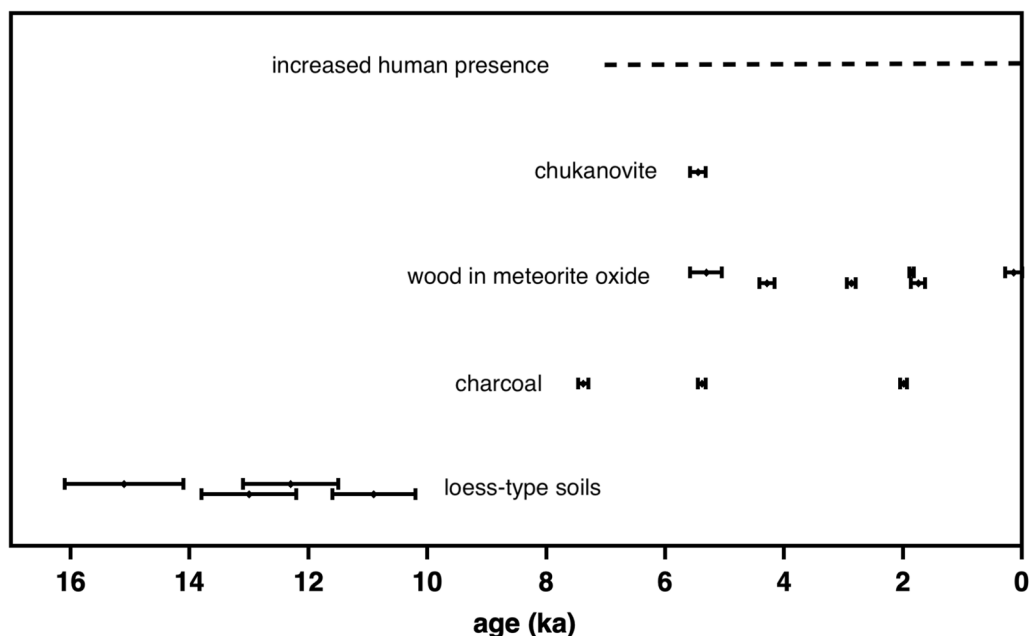### 3.4 ^{14}C ages of meteorite-associated materials

[14]C age data of meteorite-associated carbon-rich materials are shown in Table 5 and Fig. 7. Three samples of charcoal were found close to and at the same depth as meteorites, and six samples of wood inclusions in meteorite rust range from 2048 to 1929 cal BP to 7464–7294 cal BP for charcoals and sub-recent to 5575–5045 cal BP for wood. A sample of the oxidation mineral chukanovite $Fe_2CO_3(OH)_2$ from the oxidation rind of Twannberg mass TW84 yielded an age of 5582–5320 cal BP. The latter is a maximum age assuming the incorporation of carbon in equilibrium with the atmosphere at the time of formation.

4 Discussion

4.1 Meteorite distribution and association with Quaternary sediments

The areal and mass frequency distributions of meteorites on the Mont Sujet are consistent with this being a section of the essentially undisturbed strewn field with a fall direction of ∼250° from north. In contrast,

Fig. 7 New chronological constraints for loess and meteorite-associated materials. Calibrated ^{14}C ages of organic materials and the meteorite oxidation mineral chukanovite associated with Twannberg meteorites and luminescence-ages of loess-type soils on the Mont Sujet. The age evidence suggests that increased oxidation of meteorites is simultaneous with an increase in human activities based on archaeological evidence (Hafner et al., 2020)

Table 5 ^{14}C data for charcoal, wood fragments and chukanovite associated with Twannnberg meteorite finds

Sample	Coordinates	Site description	Lab code	Measurement	F^{14}C	±F^{14}C	^{14}C age (y BP)	Calendar age (95% confidence interval)	Type of analyzed material
TBP06	47° 7.830'N 7° 10.905'E	Les Prés de Macolin	BE-3649.1.1	C150723SZS	0.4467	0.0024	6473 ± 43	7464–7294 BP	Charcoal from soil, ~30 cm
TBP15	47° 7.341'N 7° 10.631'E	Gruebmatt, Twannberg	BE-3650.1.1	C150723SZS	0.5611	0.0014	4641 ± 20	5454–5313 BP	Charcoal from soil, ~45 cm
TBP16	47° 7.356'N 7° 10.548'E	Gruebmatt, Twannberg	BE-3651.1.1	C150723SZS	0.7762	0.0018	2036 ± 19	2048–1929 BP	Charcoal from soil, ~40 cm
TW84_chuk	47° 7.359'N 7° 10.630'E	Gruebmatt, Twannberg	BE-3652.1.1	C150807SZS	0.5570	0.0034	4701 ± 49	5582–5320 BP	Chukanovite, meteorite TW84
TW606	47° 7.405'N 7° 7.227'E	Mont Sujet west	BE-6944.1.1	C170421SZS	0.7886	0.0018	1908 ± 19	1892–1820 BP	Wood in meteorite oxide crust
TW677	47° 8.081'N 7° 8.286'E	Mont Sujet center	BE-6945.1.1	C170421SZS	0.6180	0.0016	3874 ± 36	4417–4161 BP	Wood in meteorite oxide crust
TW763	47° 8.408'N 7° 9.755'E	Mont Sujet east	BE-6946.1.1	C170421SZS	0.7079	0.0016	2775 ± 19	2943–2796 BP	Wood in meteorite oxide crust
TW828	47° 7.220'N 7° 7.224'E	Mont Sujet west	BE-6947.1.1	C170421SZS	0.9815	0.0022	150 ± 18	281- -5 BP	Wood in meteorite oxide crust
TW1655	47° 8.418'N 7° 8.658'E	Mont Sujet center	BE-17685.1.1	C220318SZS	0.7947	0.0037	1846 ± 39	1865–1626 BP	Wood in meteorite oxide crust
TW1715	47° 8.804'N 7° 10.042'E	Mont Sujet northeast	BE-17686.1.1	C220309GSG	0.5634	0.0056	4610 ± 80	5575–5045 BP	Wood in meteorite oxide crust

meteorites on the Twannberg plateau must be transported because their find locations and mass frequency distribution are inconsistent with the strewn field documented on the Mont Sujet. They can be derived from the same strewn field if their location of fall is assumed ~4–10 km west to southwest of the find location. Based on the close association of the Twannberg plateau meteorites with pre-LGM till, the 176 ± 19 ka (MIS 6) fall age and the general ice flow from southwest to northeast inferred from Alpine drift derived by the Valais glacier, we propose that the meteorites on the Twannberg plateau have been supraglacially transported from southwest to northeast over a distance of several kilometers during the MIS 6. The occurrence of a meteorite with preserved fusion crust in till on the Twannberg plateau demonstrates absence of mechanical wear, which is only possible when the meteorites were supraglacially, and not subglacially, transported. The glacial transport of meteorites on the Twannberg plateau and around the Mont Sujet shows that the surface of the Valais glacier during the fall must have been at least 170 m higher than during the LGM.

For an additional framework to the meteorite finds in the context of glacial materials in the Swiss Jura mountains, we show key information on topographic profiles oriented southwest-northeast (Fig. 8a, b). The widespread occurrence of Alpine drift, including the dated boulders, up to ~400 m above the highest level of LGM is evident.

Glacially transported meteorites occur at an altitude of up to 1090 m a.s.l. or ~200 m above the LGM elevation.

The mixed occurrence of meteorites and Alpine clasts in the western part of the Mont Sujet (Fig. 1b) indicates that these meteorites likely fell on the surface of the Valais glacier, but were not transported over significant distances due to a barrier function of the Chasseral and Sujet anticlines. In the northeast of the Mont Sujet, the lowest meteorite finds are in an area also containing Alpine drift (altitudes 1045–1100 m a.s.l.), likely representing glacially-transported meteorites, also indicated by the relatively large mass of some of these finds relative to the position in the strewn field. The local ice caps on the Mont Sujet and Chasseral are considered relatively stagnant while flowing Alpine ice transported meteorites from southwest to northeast and around the northeastern flank of the Mont Sujet.

The distribution of Alpine drift on the eastern part of the Chasseral anticline (area of Jobert boulder, Fig. 1b) shows a similar pattern as on the Mont Sujet, i.e. an increase of the maximum altitude from 1180 to 1320 m a.s.l. from the central part to the eastern flank.

4.2 Surface exposure ages

The large erratic boulder southeast of the Jobert farm is close to the highest altitude of Alpine material. Our new exposure age of 63 ± 1 ka for this boulder fits in an age cluster of previously-dated (Graf et al., 2015) boulders at
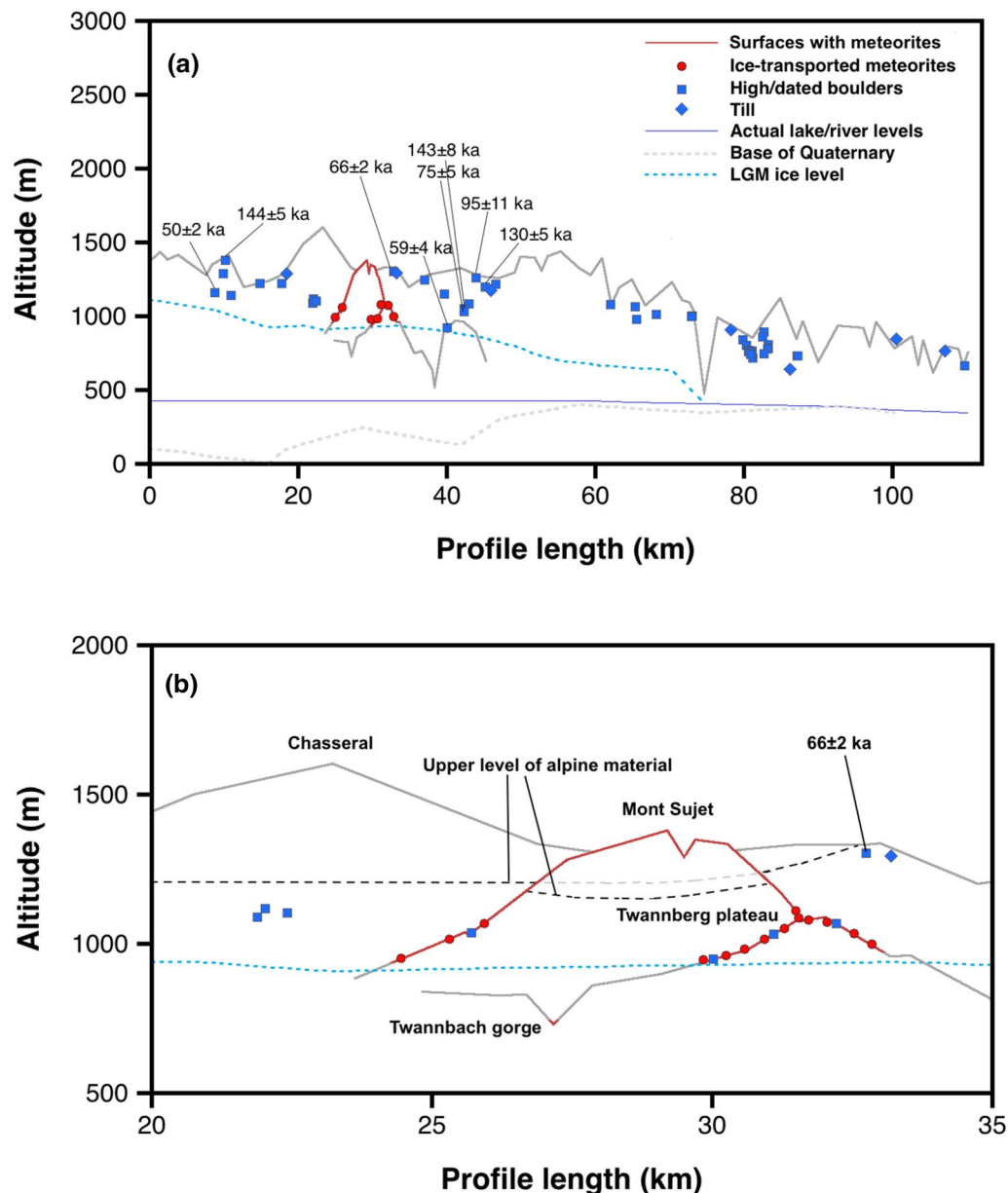
Fig. 8 **a** Topographic profile (projection on red profile line of Fig. 1a, b of the main chain of the Jura Mountains between the Mont Racine W of Neuchâtel and Dreierberg NE of Aarau, showing highest mountain crests, top of LGM ice (based on Schlüchter, 2009), Quaternary erosion level (Swisstopo), pre-LGM glacial boulders (blue squares) with exposure ages (Graf et al., 2015, this work) and pre-LGM till (blue diamonds). Topographic profiles with meteorites are shown in red, with glacially transported meteorites as red symbols. **b** Detail of Fig. 7a showing the area of the Chasseral, Mont Sujet and Twannberg plateau. Altitude of the highest occurrence of Alpine material is increased at the eastern and western flank of the Mont Sujet and at the western end of the Chasseral chain

similar altitudes (ages shown in Fig. 8a, b). These exposure ages of high boulders range from 50 ± 2 to 144 ± 5 ka and are explained by a transport of the boulders from the internal Alps during MIS 6, followed by a period of burial under ice and/or/sediment at variable depths and a subsequent differential exhumation that resulted in the exposure of boulders at different times (cf. Akçar et al., 2011).

Transport during an earlier glaciation is also possible because these exposure ages are minimum ages, but there are currently no geomorphological or geochronological constraints supporting a pre-MIS 6 deposition for these erratic boulders. We infer that the Valais glacier reached a minimal altitude of 1320 m a.s.l. (highest elevation for Alpine clasts) near the Jobert farm during the MIS

6, ~400 m higher than during the LGM. This implies that most of the Mont Sujet was covered by Alpine ice during the maximum of MIS 6 glaciations. The Twannberg meteorite fall must have occurred during a subsequent lower level of the Alpine ice surface at 1130–1200 m at the Mont Sujet. A summary of arguments for minimum ice surface during the fall of the Twannberg meteorite is given in Table 6. Based on transported meteorites beyond the maximum LGM ice extension, we have strong arguments (Table 6, arguments 1–2) that the ice-surface level during the fall was at least at 1130 m a.s.l. but not higher than ~1250 m a.s.l. in the central southern part of the Mont Sujet. If the Jobert boulder and other high-lying boulders (Graf et al., 2015) were deposited during MIS 6, the Twannberg fall must have occurred during a subsequent lower ice level, otherwise the primary strewnfield would not have been preserved at altitudes >1250 m a.s.l. on the Mont Sujet (Table 6, argument 3).

4.3 Luminescence ages of loess-type soils

The only sediments found on the Mont Sujet younger than the scattered Alpine pebbles are decarbonated loess-type soils, up to 0.5 m thick, overlying the regolith of Upper Jurassic limestone. Our luminescence ages of 10.9–15 ka demonstrate that these loess-type soils postdate the LGM (i.e. most probably Lateglacial aeolian sediment transport and deposition; e.g. Martignier et al., 2015) and are much younger than the meteorite fall, consistent with the interpretation of similar soils at other locations in the Jura Mountains as post-LGM loess (Martignier et al., 2015) or elsewhere in the internal Alps (Serra et al., 2021). The presence of some meteorites embedded in these soils must be explained by mixing with underlying meteorite-bearing limestone regolith followed by decarbonatisation, or by soil creep or pedoturbation as also revealed by young luminescence ages (<10 ka, Table 3). The occurrence of limestone-derived

oxidized pyrite in these soils also supports this interpretation.

4.4 ^{14}C ages of meteorite-associated materials

The ^{14}C ages of charcoals associated with meteorite finds, of chukanovite in a meteorite alteration crust on the Twannberg plateau, and of wood remnants embedded in meteorite oxide on the Mont Sujet range from sub-recent to 7464–7294 cal BP. These ages and the lack of older ones indicate that significant meteorite oxidation and surficial reworking took place during the last ~7300 years, possibly a result of increased wildfires (Tinner et al., 2005) and human activities including deforestation, connected with significant populations present on the nearby shores of the lakes of Biel and Neuchâtel beginning ~7000 BP (Hafner et al., 2020).

5 Summary and conclusions

The distribution of Twannberg meteorites, fallen at 176 ± 19 ka during MIS 6, the evidence of transport of meteorites by pre-LGM Alpine ice at altitudes up to ~170 m above LGM ice levels and the exposure ages of high-lying glacial boulders in the area all indicate that the level of Alpine ice during MIS 6 was up to 400 m higher than during the LGM. The Most Extensive Glaciation (MEG) was recently dated to 500 ± 100 ka (Dieleman et al., 2022). Consequently, the largest extent and probably highest ice surface of the Valais glacier can be attributed to the MEG. Based on this and our new data, we conclude that the Alpine glaciers during the MIS 6 may have reached a similar extension as the MEG glaciers.

We find no evidence for a significant lateral movement of meteorites during the LGM. Meteorites "floating" in luminescence-dated post-LGM loess-type soils indicate significant pedoturbation. Direct ^{14}C dating of meteorite oxidation using chukanovite and rust-enclosed wood, and ^{14}C dated charcoal associated with

---

Table 6 Ice surface levels at the time of the Twannberg fall

Argument 1: Ice-transported meteorites associated with till/alpine clasts west of Hohmatt (47° 8.10′N 7° 11.38′E) at an altitude of 1070 m a.s.l
Conclusion: MIS 6 ice surface level was at least 1090[1] m a.s.l., 160 m higher than during the LGM
Rating: Very strong argument, no other interpretation appears possible

Argument 2: Ice-transported meteorites associated with till/alpine clasts northeast of Mt. Sujet at altitudes of 1040 to 1090 m in the valley of Les Prés-d'Orvin (47° 8.940′N 7° 10.0′E)
Conclusion: MIS 6 ice surface level was at least 1130[1] m a.s.l., 200 m higher than during the LGM
Rating: Very strong argument. If glacial transport would have occurred along the north flank of Mt. Sujet, a higher ice level would be required

Argument 3: Jobert boulder and nearby alpine clasts (47° 9.882′N 7° 10.696′E)
Conclusion: Maximum ice level reached at least 1330[1] m a.s.l., 400 m higher than during LGM. If this happened during MIS 6 as is indicated by exposure ages[2], the Twannberg fall must have occurred after glacial maximum at a time when the ice surface level was lower than ~1250 m a.s.l. based on the preservation of the primary distribution of meteorites on Mont Sujet
Rating: Argument depends on the transport age of the Jobin boulder and other high-lying boulders[2], a transport prior to MIS 6 is possible

---

[1] All estimated ice surface levels are given for a position in the center of the south flank of Mt. Sujet, 47° 7.7′ N 7° 8.7′E, assuming an eastward ice slope of 7‰. The local ice level during the LGM at this position was ~930 m (Schlüchter 2009, Aufranc & Burkhalter, 2017)

[2] Graf et al. (2015)

meteorite finds demonstrate increased meteorite oxidation during the last ~ 7300 years, related to locally enhanced vegetation burning and erosion both on the Mont Sujet and on the Twannberg plateau, probably coincident with an increase in human activities in the area concurrent with the first Neolithic settlements in the area around 7000 BP (Hafner et al., 2020).

Supplementary Information

The online version contains supplementary material available at https://doi.org/10.1186/s00015-023-00442-3.

> **Additional file 1: Material S1.** Terrestrial age of the Twannberg meteorite based on cosmogenic isotopes. **Material S2.** Determination of the fall direction of the Twannberg meteorite. **Material S3.** Exposure age of the glacial boulder at Ferme Jobert: Sampling documentation.

Declarations

Author details

[1]Naturhistorisches Museum Bern, Bernastrasse 15, 3005 Bern, Switzerland. [2]Institute of Geological Sciences, University of Bern, Baltzerstrasse 1+3, 3012 Bern, Switzerland. [3]Department of Chemistry, Biochemistry and Pharmaceutical Sciences and Oeschger Centre for Climate Change Research, University of Bern, Freiestrasse 3, 3012 Bern, Switzerland. [4]Université Grenoble Alpes, CNRS, IRD, IFSTAR, ISTERRE, Université Savoie Mont Blanc, 38000 Grenoble, France. [5]Laboratory of Ion Beam Physics, Swiss Federal Institute of Technology Zurich (ETHZ), Otto-Stern-Weg 5, 8093 Zurich, Switzerland.

References

Akçar, N., Deline, P., Ivy-Ochs, S., Alfimov, V., Hajdas, I., Kubik, P. W., Christl, M., & Schlüchter, C. (2012). The AD 1717 rock avalanche deposits in the upper Ferret Valley (Italy): A dating approach with cosmogenic Be-10. *Journal of Quaternary Science, 27*, 383–392. https://doi.org/10.1002/jqs.1558

Akçar, N., Ivy-Ochs, S., Alfimov, V., Schlunegger, F., Claude, A., Reber, R., Christl, M., Vockenhuber, C., Dehnert, A., Rahn, M., & Schlüchter, C. (2017). Isochron-burial dating of glaciofluvial deposits: First results from the Swiss Alps. *Earth Surface Processes and Landforms, 42*, 2414–2425. https://doi.org/10.1002/esp.4201

Akçar, N., Ivy-Ochs, S., Kubik, P. W., & Schlüchter, C. (2011). Post-depositional impacts on "Findlinge" (erratic boulders) and their implications for surface-exposure dating. *Swiss Journal of Geosciences, 104*, 445–453. https://doi.org/10.1007/s00015-011-0088-7

Auclair, M., Lamothe, M., & Huot, S. (2003). Measurement of anomalous fading for feldspar IRSL using SAR. *Radiation Measurements, 37*, 487–492. https://doi.org/10.1016/S1350-4487(03)00018-0

Aufranc, J., & Burkhalter, R. (2017). 1125 Chasseral, Geological Atlas of Switzerland 1:25'000. Bundesamt für Landestopographie swisstopo, Wabern.

Balco, G., & Rovey, C. W. (2008). An isochron method for cosmogenic-nuclide dating of buried soils and sediments. *American Journal of Science, 308*, 1083–1114. https://doi.org/10.2475/10.2008.02

Balescu, S., & Lamothe, M. (1994). Comparison of TL and IRSL age estimates of feldspar coarse grains from waterlain sediments. *Quaternary Science Reviews, 13*, 437–444. https://doi.org/10.1016/0277-3791(94)90056-6

Bickel, L., Lüthgens, C., Lomax, J., & Fiebig, M. (2015). Luminescence dating of glaciofluvial deposits linked to the penultimate glaciation in the Eastern Alps. *Quaternary International, 357*, 110–124. https://doi.org/10.1016/j.quaint.2014.10.013

Buhl, S., & McColl, D. (2012). *Henbury craters and meteorites* (p. 166). Meteorite Recon.

Bühler, R. W. (1986). Twannberg—ein neuer Schweizer Eisenmeteorit. *Orion, 217*, 188–192.

Buylaert, J. P., Murray, A. S., Thomsen, K. J., & Jain, M. (2009). Testing the potential of an elevated temperature IRSL signal from K-feldspar. *Radiation Measurements, 44*, 560–565. https://doi.org/10.1016/j.radmeas.2009.02.007

Chmeleff, J., von Blanckenburg, F., Kossert, K., & Jakob, D. (2010). Determination of the Be-10 half-life by multicollector ICP-MS and liquid scintillation counting. *Nuclear Instruments & Methods in Physics Research Section B-Beam Interactions with Materials and Atoms, 268*, 192–199.

Christl, M., & Kubik, P. W. (2013). New Be-cathode preparation method for the ETH 6 MV Tandem. *Nuclear Instruments and Methods in Physics Research Section B: Beam Interactions with Materials and Atoms, 294*, 199–202. https://doi.org/10.1016/j.nimb.2012.03.031

Dieleman, C., Christl, M., Vockenhuber, C., Gautschi, P., Graf, H. R., & Akçar, N. (2022). Age of the most extensive glaciation in the alps. *Geosciences, 12*, 39. https://doi.org/10.3390/geosciences12010039

Dunne, J., Elmore, D., & Muzikar, P. (1999). Scaling factors for the rates of production of cosmogenic nuclides for geometric shielding and attenuation at depth on sloped surfaces. *Geomorphology, 27*, 3–11.

Durcan, J. A., King, G. E., & Duller, G. A. T. (2015). DRAC: Dose rate and age calculator for trapped charge dating. *Quaternary Geochronology, 28*, 54–61. https://doi.org/10.1016/j.quageo.2015.03.012

Folco, L., Martino, M. D., Barkooky, A. E., D'Orazio, M., Lethy, A., Urbini, S., Nicolosi, I., Hafez, M., Cordier, C., Ginneken, M. V., Zeoli, A., Radwan, A. M., Khrepy, S. E., Gabry, M. E., Gomaa, M., Barakat, A. A., Serra, R., & Sharkawi, M. E. (2011). Kamil Crater (Egypt): Ground truth for small-scale meteorite impacts on Earth. *Geology, 39*, 179–182. https://doi.org/10.1130/G31624.1

Galbraith, R. F., Roberts, R. G., Laslett, G. M., Yoshida, H., & Olley, J. M. (1999). Optical dating of single and multiple grains of quartz from jinmium rock shelter, northern Australia: Part I, experimental design and statistical models. *Archaeometry, 2*, 339–364. https://doi.org/10.1111/j.1475-4754.1999.tb00987.x

Gnos, E., Lorenzetti, S., Eugster, O., Jull, A. J. T., Hofmann, B. A., Al-Kathiri, A., & Eggimann, M. (2009). The Jiddat al Harasis 073 strewnfield, Sultanate of Oman. *Meteoritics and Planetary Science, 44*, 375–387. https://doi.org/10.1111/j.1945-5100.2009.tb00739.x

Graf, A., Akçar, N., Ivy-Ochs, S., Strasky, S., Kubik, P. W., Christl, M., Burkhard, M., Wieler, R., & Schlüchter, C. (2015). Multiple advances of Alpine glaciers into the Jura Mountains in the Northwestern Switzerland. *Swiss Journal of Earth Sciences, 108*, 225–238. https://doi.org/10.1007/s00015-015-0195-y

Graf, A. A., Strasky, S., Ivy-Ochs, S., Akçar, N., Kubik, P. W., Burkhard, M., & Schlüchter, C. (2007). First results of cosmogenic dated pre-Last Glaciation erratics from the Montoz area, Jura Mountains, Switzerland. *Quaternary International, 164–165*, 43–52. https://doi.org/10.1016/j.quaint.2006.12.022

Gruner, U., Aufranc, J., Antenen, M., & Schürch, R. (2013). Geologischer Atlas der Schweiz 1:25′000, 1126 Büren a.A., Erläuterungen. Bundesamt für Landestopographie swisstopo, Wabern.

Hafner, A., Rey, F., Hostettler, M., Laabs, J., Bolliger, M., Brombacher, C., Francuz, J., Gobet, E., Häberle, S., Rentzel, P., Schäfer, M., Schibler, J., Wey, O., & Tinner, W. (2020). Archaeological and palaeoecological investigations at Burgäschisee (Swiss Plateau): new interdisciplinary insights in Neolithic settlement, land use and vegetation dynamics. In A. Hafner, E. Dolbunova, A. Mazurkevich, E. Pranckenaite, & M. Hinz (Eds.), *Settling Waterscapes in Europe. The Archaeology of Neolithic and Bronze Age Pile-Dwellings* (pp. 173–204). Propylaeum.

Halsted, C. T., Bierman, P. R., & Balco, G. (2021). Empirical evidence for latitude and altitude variation of the in situ cosmogenic ^{26}Al/^{10}Be production ratio. *Geosciences, 11*, 402. https://doi.org/10.3390/geosciences11100402

Heim, A. (1919). *Geologie der Schweiz*. Tauchnitz.

Hofmann, B.A., Jost, M., & Koppelt, A. (2016). Der Twannberg-Eisenmeteorit, Funde 1984–2016. Space Jewels Switzerland, 108 p.

Hofmann, B. A., Lorenzetti, S., Eugster, O., Krähenbühl, U., Herzog, G., Gnos, E., Eggimann, M., & Wasson, J. T. (2009). The Twannberg (Switzerland) IIG iron meteorites: Mineralogy, chemistry and CRE ages. *Meteoritics and Planetary Science, 44*, 187–199. https://doi.org/10.1111/j.1945-5100.2009.tb00727.x

Hua, Q., Barbetti, M., & Rakowski, A. Z. (2013). Atmospheric Radiocarbon for the Period 1950–2010. *Radiocarbon, 55*, 2059–2072. https://doi.org/10.2458/azu_js_rc.v55i2.16177

Huntley, D. J., & Baril, M. R. (1997). The K content of the K-feldspars being measured in optical dating or in thermoluminescence dating. *Ancient TL, 15*, 11–13.

Huntley, D. J., & Lamothe, M. (2001). Ubiquity of anomalous fading in K-feldspars and the measurement and correction for it in optical dating. *Canadian Journal of Earth Sciences, 38*, 1093–1106. https://doi.org/10.1139/e01-013

Ivy-Ochs, S. (2015). Glacier variations in the European Alps at the end of the last glaciation. *Cuadernos De Investigacion Geografica, 41*, 295–315.

Kofmann, R. S., Herd, C. D. K., & Froese, D. G. (2010). The Whitecourt meteorite impact crater, Alberta, Canada. *Meteoritics and Planetary Science, 45*, 1429–1445. https://doi.org/10.1111/j.1945-5100.2010.01118.x

Kohl, C. P., & Nishiizumi, K. (1992). Chemical isolation of quartz for measurement of insitu-produced cosmogenic nuclides. *Geochimica et Cosmochimica Acta, 56*, 3583–3587.

Korschinek, G., Bergmaier, A., Faestermann, T., Gerstmann, U. C., Knie, K., Rugel, G., Wallner, A., Dillmann, I., Dollinger, G., von Gostomski, C. L., Kossert, K., Maiti, M., Poutivtsev, M., & Remmert, A. (2010). A new value for the half-life of Be-10 by Heavy-Ion Elastic Recoil Detection and liquid scintillation counting. *Nuclear Instruments & Methods in Physics Research Section B-Beam Interactions with Materials and Atoms, 268*, 187–191.

Kreutzer, S., Schmidt, C., Fuchs, M., & Dietze, M. (2012). Introducing an R package for luminescence dating analysis. *Ancient TL, 30*, 1–8.

Kring, D. A., Jull, A. J. T., McHargue, L. R., Bland, P. A., Hillegonds, D. J., & Berry, F. J. (2001). Gold Basin meteorite strewn field, Mojave Desert, northwestern Arizona: Relic of a small late Pleistocene impact event. *Meteoritics and Planetary Science, 36*, 1057–1066. https://doi.org/10.1111/j.1945-5100.2001.tb01944.x

Krinov, E. L. (1974). Fragmentation of the Sikhote-Alin meteoritic body. *Meteoritics, 9*, 255–262.

Kubik, P. W., & Christl, M. (2010). ^{10}Be and ^{26}Al measurements at the Zurich 6 MV Tandem AMS facility. *Nuclear Instruments and Methods in Physics Research Section B: Beam Interactions with Materials and Atoms, 268*, 880–883. https://doi.org/10.1016/j.nimb.2009.10.054

Martignier, L., Nussbaumer, M., Adatte, T., Gobat, J.-M., & Verrecchia, E. P. (2015). Assessment of a locally-sourced loess system in Europe: The Swiss Jura Mountains. *Aeolian Research, 18*, 11–21. https://doi.org/10.1016/j.aeolia.2015.05.003

Murray, A. S., & Wintle, A. G. (2000). Dating quartz using an improved single-aliquot regenerative-dose (SAR) protocol. *Radiation Measurements, 32*, 57–73. https://doi.org/10.1016/S1350-4487(99)00253-X

Nishiizumi, K. (2004). Preparation of Al-26 AMS standards. *Nuclear Instruments & Methods in Physics Research Section B-Beam Interactions with Materials and Atoms, 223*, 388–392.

Norris, T. L., Gancarz, A. J., Rokop, D. J., & Thomas, K. W. (1983). Half-Life of Al-26. *Journal of Geophysical Research, 88*, B331–B333.

Popova, O. P., Jenniskens, P., Emel'yanenko, V., Kartashova, A., Biryukov, E., Khaibrakhmanov, S., Shuvalov, V., Rybnov, Y., Dudorov, A., Grokhovsky, V. I., Badyukov, D. D., Yin, Q.-Z., Gural, P. S., Albers, J., Granvik, M., Evers, L. G., Kuiper, J., Kharlamov, V., Solovyov, A., … Mikouchi, T. (2013). Chelyabinsk airburst, damage assessment, meteorite recovery, and characterization. *Science, 342*, 1069–1073. https://doi.org/10.1126/science.1242642

Preusser, F., & Kasper, H. U. (2001). Comparison of dose rate determination using high-resolution gamma spectrometry and inductively coupled plasma-mass spectrometry. *Ancient TL, 19*, 17–21.

Reimer, P. J., Austin, W. E. N., Bard, E., Bayliss, A., Blackwell, P. G., Bronk Ramsey, C., Butzin, M., Cheng, H., Edwards, R. L., Friedrich, M., Grootes, P. M., Guilderson, T. P., Hajdas, I., Heaton, T. J., Hogg, A. G., Hughen, K. A., Kromer, B., Manning, S. W., Muscheler, R., … Talamo, S. (2020). The IntCal20 northern hemisphere radiocarbon age calibration curve (0–55 cal kBP). *Radiocarbon, 62*, 725–757. https://doi.org/10.1017/RDC.2020.41

Schlüchter, C. (compil)(2009). Die Schweiz während des letzteiszeitlichen Maximums (LGM): 1:500 000, Bundesamt für Landestopografie, swisstopo. Wabern, Switzerland.

Serra, E., Valla, P. G., Gribenski, N., GuedesMagrani, F., Carcaillet, J., Delaloye, R., Grobety, B., & Braillard, L. (2021). Geomorphic response to the lateglacial-eholocene transition in high alpine regions sanetsch pass, Swiss Alps. *Boreas, 50*, e242–e261.

Smith, T., Cook, D. L., Merchel, S., Pavetich, S., Rugel, G., Scharf, A., & Leya, I. (2019). The constancy of galactic cosmic rays as recorded by cosmogenic nuclides in iron meteorites. *Meteoritics and Planetary Science, 54*, 2951–2976. https://doi.org/10.1111/maps.13417

Smith, T., Hofmann, B. A., Leya, I., Merchel, S., Pavetich, S., Rugel, G., & Scharf, A. (2017). The cosmic-ray exposure history of the Twannberg iron meteorite (IIG). *Meteoritics and Planetary Science, 52*, 2241–2257. https://doi.org/10.1111/maps.12928

Szidat, S., Salazar, G. A., Vogel, E., Battaglia, M., Wacker, L., Synal, H.-A., & Türler, A. (2014). ^{14}C analysis and sample preparation at the new Bern Laboratory for the Analysis of Radiocarbon with AMS (LARA). *Radiocarbon, 56*, 561–566. https://doi.org/10.2458/56.17457

Tinner, W., Conedera, M., Ammann, B., & Lotter, A. F. (2005). Fire ecology north and south of the Alps since the last ice age. *The Holocene, 15*, 1214–1226.

Wasson, J. T., & Choe, W.-H. (2009). The IIG iron meteorites: Probable formation in the IIAB core. *Geochimica et Cosmochimica Acta, 73*, 4879–4890. https://doi.org/10.1016/j.gca.2009.05.062

Publisher's Note